Journal of Biomedical Optics

SPIEDigitalLibrary.org/jbo

Integrated micro-endoscopy system for simultaneous fluorescence and optical-resolution photoacoustic imaging

Peng Shao
Wei Shi
Parsin Hajireza
Roger J. Zemp

SPIE

Integrated micro-endoscopy system for simultaneous fluorescence and optical-resolution photoacoustic imaging

Peng Shao, Wei Shi, Parsin Hajireza, and Roger J. Zemp
University of Alberta, Department of Electrical and Computer Engineering, Edmonton, Alberta, T6G 2V4, Canada

Abstract. We present a new integrated micro-endoscopy system combining label-free, fiber-based, real-time C-scan optical-resolution photoacoustic microscopy (F-OR-PAM) and a high-resolution fluorescence micro-endoscopy system for visualizing fluorescently labeled cellular components and optically absorbing microvasculature simultaneously. With a diode-pumped 532-nm fiber laser, the F-OR-PAM sub-system is able to reach a resolution of ~7 μm. The fluorescence subsystem, which does not require any mechanical scanning, consists of a 447.5-nm-centered diode laser as the light source, an objective lens, and a CCD camera. Proflavine is used as the fluorescent contrast agent by topical application. The scanning laser and the diode laser light source share the same light path within an optical fiber bundle containing 30,000 individual single-mode fibers. The absorption of proflavine at 532 nm is low, which mitigates absorption bleaching of the contrast agent by the photoacoustic excitation source. We demonstrate imaging in live murine models. The system is able to provide cellular morphology with cellular resolution co-registered with the structural information given by F-OR-PAM. Therefore, the system has the potential to serve as a virtual biopsy technique, helping visualize angiogenesis and the effects of anti-cancer drugs on both cells and the microcirculation, as well as aid in the study of other diseases. [DOI: 10.1117/1.JBO.17.7.076024]

Keywords: optical-resolution photoacoustic microscopy; fluorescent microscopy.

Paper 12194P received Mar. 25, 2012; revised manuscript received Jun. 21, 2012; accepted for publication Jun. 25, 2012; published online Jul. 18, 2012.

1 Introduction

Optical-resolution photoacoustic microscopy (OR-PAM) is capable of sensing endogenous optical absorption in biological bodies with fine lateral resolution provided by optical focusing. Pioneered by Maslov et al.,[1] OR-PAM imaging has been successfully applied to both structural and functional imaging.[2–9] Since both oxy- and deoxyhemoglobin are the dominant absorbing components in blood, the distribution of optical absorption, detected by the OR-PAM system, can be used to recover oxygen saturation (SO_2). For example, Hu et al.[10] used OR-PAM to image SO_2 with capillary-level resolution in mouse brain with dual-wavelength measurements. Hu et al.[11] also imaged the healing process of laser-induced microvascular lesions in a small animal model *in vivo* in terms of morphological and SO_2 mapping. These studies demonstrated the capability of OR-PAM as a potential powerful tool in microcirculatory physiology and pathophysiology.

Recently our group reported the first label-free, fiber-based OR-PAM (F-OR-PAM) imaging systems.[12,13] The system retains many of the powerful properties of our previously proposed table-top system.[14] It takes advantage of a flexible image guide and has significant potential to serve as a new micro-endscopic imaging technique for clinical use. Visualization of microvasculature in living mouse ears was demonstrated with the system.

Fluorescence contrast high-resolution fiber-optic micro-endoscopy (HRME) was introduced by Muldoon et al.[15] This technique, which is inspired by the goal of virtual histopathology, utilizes a microscopic setup to image fluorescently-labelled cellular structures with lateral resolution on the order of microns. Fluorescent signals excited by a wide-field light source are magnified and sensed by a CCD camera. Rosbach et al.[16] justified the feasibility of the imaging modality in evaluating lymph nodes from breast cancer patients with morphological variation. Muldoon et al.[17] verified the validity of the technique in assisting diagnosis of oral lesions by observing and analyzing morphology of epithelia in human oral cavities.

In the present paper, we propose a combined system based on the HRME technique and our previous F-OR-PAM system, with the purpose of engineering a hybrid imaging platform to visualize capillary vasculatures along with cellular context.

2 Methods

The dual modality imaging platform consists of two modules (Fig. 1). The F-OR-PAM system employs a 532-nm diode-pumped Ytterbium-doped fiber laser system as the optical source (GLP-10, IPG Photonics Corporation). Pulse repetition rate (PRR) of the laser system is tunable within the range from 20 k to 600 kHz. Pulse duration is ~1 ns and the pulse energy can reach up to 20 μJ. A pair of 2D galvanometer scanning mirrors (6230H, Cambridge Technology, Inc.) is utilized to accomplish optical scanning. The scanners are driven by two analog sinusoidal waves (x- and y-direction) from a function generator. The scanned beam is then focused by an objective lens ($f = 18$ mm, K16033703, Mitutoyo Co.) and directed into an image-guide fiber (FIGH-30-850, Myriad Fiber Imaging Tech., Inc.). Photoacoustic signals are sensed by a 3.5-MHz transducer (19-mm focus, 6-mm active element, f#=3.17, CD International Technology, Inc.), amplified, and pre-filtered by

Address all correspondence to: Roger J. Zemp, University of Alberta, Department of Electrical and Computer Engineering, Edmonton, Alberta, T6G 2V4, Canada. Tel: 780-902-9463; Fax: 780 492 1811; E-mail: rzemp@ualberta.ca

0091-3286/2012/$25.00 © 2012 SPIE

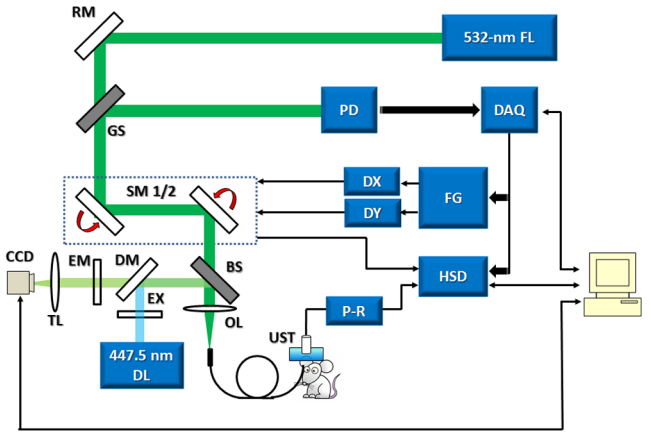

Fig. 1 Experimental setup for the combined photoacoustic and fluorescence micro-endoscopy imaging system (RM: reflective mirror; GS: glass slide; PD: photodiode; SM1/2: scanning mirrors 1 and 2; FG: function generator; DX/Y: galvanometer scanning mirror divers; BS: beam splitter; OL: objective lens; UST: ultrasound transducer; P-R: pulser-receiver; TL: tube lens; EM: emission filter; DM: dichroic mirror; EX: excitation filter; DL: diode laser; DAQ: data acquisition card; HSD: high-speed digitizer; FL: fiber laser). The system is composed of an OR-PAM subsystem and a fluorescence microscopy system. A 2D galvanometer scanning mirror pair is used for raster optical scanning of the focused laser pulse. In the fluorescence imaging subsystem, excitation light is selected with an excitation filter and a dichroic mirror and directed by a beam splitter to share the same light path as the laser beam through the objective lens and the image guide to the target. Fluorescence energy is then reflected back through the dichroic mirror and then focused by a tube lens to the high-resolution CCD camera.

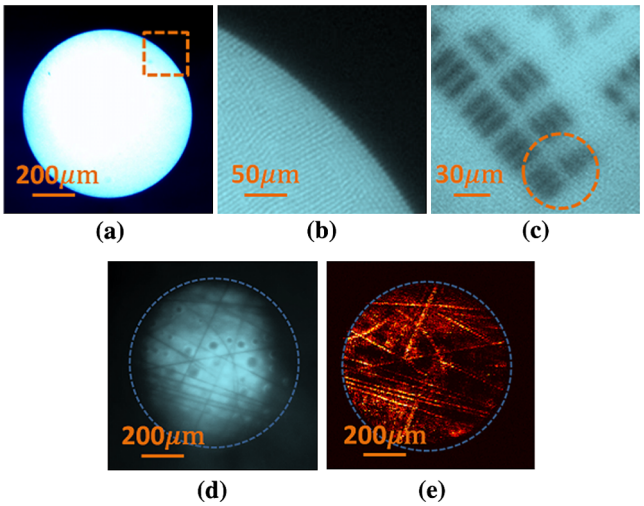

Fig. 2 System characterization. Panel (a) is the whole footprint of the image guide, with a diameter of ~800 μm Panel (b) is a zoomed-in version of the region in the dashed rectangle in (a). When the imaging system is well focused, single elements of the image guide can be visualized. Panel (c) is the image of the USAF 1951 resolution target taken with the fluorescent imaging system. Bars with a width of around 4.38 μm are resolved. Panels (d) and (e) are the same carbon fiber network imaged with the fluorescent imaging module and the F-OR-PAM module sequentially. Consistent contents are visualized in the two images.

a pulser-receiver (5900 PR, Olympus NDT, Inc.) and then digitized by a 12-bit, 8-channel, high-speed digitizer (CS8289, Gage Applied Technologies, Inc.) along with the higher-frequency (x-axis) scanning feedback signals. For the fluorescent sub-system, a 447.5-nm-centered diode laser is utilized as the excitation light source. A standard fluorescent filter unit is employed in the system. An exciter band-pass filter with a center wavelength (Thorlabs, Inc.) of 445 nm is utilized. A 475-nm cut-off dichroic mirror (Chroma Technology Corp.) is used to reflect excitation light while transmitting excited fluorescence signals back. Excited fluorescence signals travel back through the image guide, reflected by the beam splitter positioned above the objective lens, and then follow the light path to the scientific-grade, high-resolution Electron-Multiplied CCD (EM-CCD, Andor iXon 885, Andor Technology). To rule out noise in the fluorescence signals, we use a 500-nm long-pass barrier filter (Thorlabs, Inc.) between dichroic mirror and tube lens. Pixel size of the CCD is $8\ \mu m \times 8\ \mu m$ and there are 1002×1004 pixels in total. The objective lens and the tube lens function together as a microscopic system. We use a plano-convex lens with a focal length of 150 mm (Thorlabs, Inc.) as the tube lens and therefore the magnification factor of the system is ~8.3. Proflavine, an FDA-approved drug for human medical use, is utilized as the contrast agent. In soft tissue, proflavine stains nuclei. This is important, since nuclei are often enlarged in cancer cells. Since the 532-nm laser is away from the absorption spectrum of Proflavine, no fluorescence signals will be generated by our OR-PAM optical source.

The image guide we used, which consists of 30,000 single-mode fibers in a bundle, has a diameter of ~800 μm. Considering the magnification factor of the microscope system, each single fiber covers 4.7 pixels of the EM-CCD on average, which is above the Nyquist limit.

The software package for data acquisition and data transfer is written in C/C++, and data processing and analysis is conducted with Matlab (Mathworks, Inc.).

3 Results

3.1 *System Characterization*

Figure 2 illustrates the system characterization of the imaging system. Figure 2(a) shows the entire footprint of the image guide we use, which has a diameter of ~800 μm. When the fluorescent imaging module is well focused, single elements of the image guide can be visualized, as is shown in Fig. 2(b). This demonstrates that the module is capable of imaging features at a cellular level. To examine the lateral resolution of the fluorescent module, we imaged a 1951 United Stated Air Force resolution target (USAF 1951). Features with a dimension of 4.38 μm can be resolved, which suggests that the imaging module has a lateral resolution that is on the order of the F-OR-PAM subsystem. For properties of our F-OR-PAM module, readers can refer to Ref. 12 for details. Figure 2(d) and 2(e) are images of a carbon fiber network obtained with both the two modules with fluorescent dye applied to the background. Contents in the two images are consistent. While carbon fibers appear as dark features in the fluorescent images, the F-OR-PAM image relies on photoacoustic signals from the fiber structures. The dual-modality imaging platform is capable of simultaneously providing two kinds of information that are supplementary to each other.

3.2 *In Vivo Imaging*

In vivo studies were conducted to demonstrate imaging capability of our system. An ear of a 7-week-old SCID hairless outbred

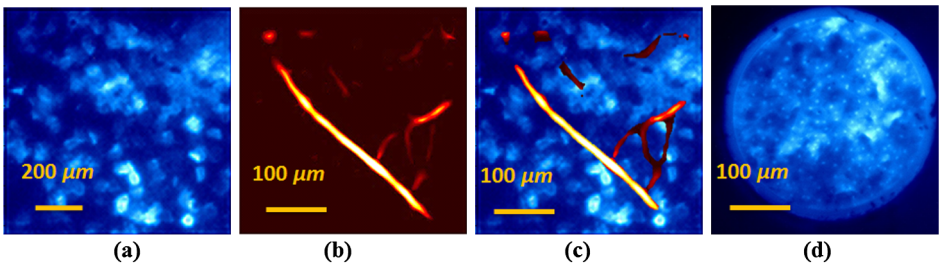

Fig. 3 Results of *in vivo* experiments. Panel (a) is the fluorescence image of the mouse ear taken at the same location where the F-OR-PAM image was obtained; panel (b) is the F-OR-PAM image. (c) Co-registered image of (a) and (b). (d) Fluorescence image of normal human oral mucosa with topical application of Proflavine.

mouse was imaged for *in vivo* studies. Experimental procedures followed the laboratory animal protocol approved by the University of Alberta Animal Use and Care Committee. An animal anesthesia system was utilized while image data were collected. Before the imaging experiment, we topically applied proflavine-saline solution with a concentration of 0.01% (w/v) to the ear skin surface. To avoid contamination of fluorescence image by our fiber laser, the fluorescent and F-OR-PAM images were taken sequentially in a few minutes after the dye was applied. But acquisition of the two images can be interlaced. The measured power of the excitation 455-nm light at distal end of the image guide is around 0.45 mW. The 532-nm laser works with PRR of 160 kHz. The average power measured at the distal end when conducting F-OR-PAM imaging is around 35 mW. Results of the experiment are shown in Fig. 3. The scanning frequency of the galvanometer mirror system is 400 Hz and 1 Hz for the *x*- and *y*-axis, respectively. With the laser repetition rate of 160 kHz, the frame rate of the F-OR-PAM imaging subsystem is two frames per second, resulting in images with 160,000 points. Figure 3(a) and 3(b) are the F-OR-PAM maximum amplitude projection (MAP) and fluorescent images of the mouse ear obtained at the same location, respectively. A two dimensional Hessian-based Frangi vesselness filter was used for data processing.[18] Figure 3(c) is the coregistered image.

Figure 3(d) is a fluorescence image of normal human oral mucosa taken with our system. After topical application of the fluorescent dye, the distal end of the image guide was placed in contact with normal human oral mucosa to acquire fluorescent images. Staining of nuclei and cell membrane can be visualized clearly in the image.

4 Discussion

We demonstrated a hybrid imaging system for both F-OR-PAM-based vasculature and fluorescently labeled cellular structure imaging. We further provide cellular information on the micron scale based on the OR-PAM system reported by our group.[12,13] We believe that the concept shown in the present paper may lead to a more powerful tool for biomedical imaging.

A potential application of our system is the study and diagnosis of early-stage cancer. Whereas F-OR-PAM can provide images of vasculature (and potentially hemoglobin oxygenation) in tissue, cellular information may provide morphological context, which is crucial for researchers and clinicians. For example, morphological anomalies in tumor tissue and variations in the microvasculatures due to cancer angiogenesis can confirm each other. This enables the technique to serve as a form of noninvasive virtual biopsy for identification of superficial tumor tissues in human cavities in diagnosis by clinicians. Estimate of SO_2 at capillary level, which is not possible with pure fluorescence imaging, can also be accomplished with dual-wavelength OR-PAM imaging.[10] This could help reveal the metabolic status of the cancer tissue, which is proven to be of importance for both fundamental studies and clinical practices. Another example is vasa vasorum imaging. Angiogenesis in this vascular layer of the lumen of atherosclerotic vessels has been correlated with plaque vulnerability. Visualizing the vessels could help provide one determinant of plaque vulnerability while fluorescent labeling could target immune cell invasion as an additional surrogate measure of rupture vulnerability.

We would like to note that though the fluorescent dye we use for the present project is not cell specific, various dye materials can be utilized to label different cells, cell markers, or subcellular features in the soft tissue to generate contrast between tissue components—for example, the amine-reactive derivatives of fluorescein isothiocyanate (FITC), which is widely used for various applications such as antibody labeling in immunofluorescence. The FDA-approved dye indocyanine green (ICG)[19,20] has the advantage of near-infrared excitation and could also be considered as a myriad of existing and emerging fluorescent reporters. Investigation of these dyes is warranted in our future work for novel potential applications.

Acknowledgments

We gratefully acknowledge funding from the Canadian Cancer Society (TFF 019237, TFF 019240, CCS 2011-700718), NSERC (355544-2008, 375340-2009, STPGP 396444), the Terry Fox Foundation, the Alberta Cancer Research Institute (ACB 23728), the Canada Foundation for Innovation Leaders Opportunity Fund (18472), Alberta Advanced Education & Technology Small Equipment Grants Program (URSI09007-SEG), Microsystems Technology Research Initiative (MSTRI RES0003166), and University of Alberta Startup Funds. We also acknowledge student scholarship support from Alberta Ingenuity, Alberta Innovates, NSERC, and the China Scholarship Council.

References

1. K. Maslov et al., "Optical-resolution photoacoustic microscopy for in vivo imaging of single capillaries," *Opt. Lett.* **33**(9), 929–931 (2008).
2. S. Hu, K. Maslov, and L. V. Wang, "Noninvasive label-free imaging of microhemodynamics by optical-resolution photoacoustic microscopy," *Opt. Express* **17**(9), 7688–7963 (2009).
3. H. F. Zhang et al., "Functional photoacoustic microscopy for high-resolution and noninvasive in vivo imaging," *Nat. Biotech.* **24**(7), 848–851 (2006).

4. S. Hu, K. Maslov, and L. V. Wang, "In vivo functional chronic imaging of a small animal model using optical-resolution photoacoustic microscopy," *Med. Phys.* **36**(6), 2320–2323 (2009).
5. L. Song, K. Maslov, and L. V. Wang, "Multifocal optical-resolution photoacoustic microscopy in vivo," *Opt. Lett.* **36**(7), 1236–1238 (2011).
6. J. Yao et al., "In vivo photoacoustic imaging of transverse blood flow by using Doppler broadening of bandwidth," *Opt. Lett.* **35**(9), 1419–1421 (2010).
7. V. Tsytsarev et al., "Photoacoustic microscopy of microvascular responses to cortical electrical stimulation," *J. Biomed. Opt.* **16**(7), 076002 (2011).
8. A. Krumholz et al., "Photoacoustic microscopy of tyrosinase reporter gene in vivo," *J. Biomed. Opt.* **16**(8), 080503 (2011).
9. B. Rao et al., "Real-time four-dimensional optical-resolution photoacoustic microscopy with Au nanoparticle-assisted subdiffraction-limit resolution," *Opt. Lett.* **36**(7), 1137–1139 (2011).
10. S. Hu et al., "Functional transcranial brain imaging by optical-resolution photoacoustic microscopy," *J. Biomed. Opt.* **14**(4), 040503 (2009).
11. S. Hu, K. Maslov, and L. V. Wang, "In vivo functional chronic imaging of a small animal model using optical-resolution photoacoustic microscopy," *Med. Phys.* **36**(6), 2320–2323 (2009).
12. P. Hajireza, W. Shi, and R. J. Zemp, "Label-free in vivo fiber-based optical-resolution photoacoustic microscopy," *Opt. Lett.* **36**(20), 4107–4109 (2011).
13. P. Hajireza, W. Shi, and R. J. Zemp, "Real-time handheld optical-resolution photoacoustic microscopy," *Opt. Express* **19**(21), 20097–20102 (2011).
14. W. Shi et al., "In vivo near-realtime volumetric optical-resolution photoacoustic microscopy using a high-repetition-rate nanosecond fiber-laser," *Opt. Express* **19**(18), 17143–17150 (2011).
15. T. J. Muldoon et al., "Subcellular-resolution molecular imaging within living tissue by fiber microendoscopy," *Opt. Express* **15**(25), 16413–16423 (2007).
16. K. J. Rosbach et al., "High-resolution fiber optic microscopy with fluorescent contrast enhancement for the identification of axillary lymph node metastases in breast cancer: a pilot study," *Biomed. Opt. Express* **1**(3), 911–922 (2010).
17. T. J. Muldoon et al., "Noninvasive imaging of oral neoplasia with a high-resolution fiber-optic microscope," *Head Neck* **34**(3), 305–312 (2012).
18. R. Manniesing and W. Niessen, "Multiscale vessel enhancing diffusion in CT angiography noise filtering," in *Lecture Notes in Computer Science*, Vol. **3565**, pp. 138–149, Springer, Berlin Heidelberg New York (2005).
19. M. Miwa, "The principle of ICG fluorescence methods," *Open Surg. Oncol. J.* **2**, 26–28 (2010).
20. M. Ogawa et al., "In vivo molecular imaging of cancer with a quenching near-infrared fluorescence probe using conjugates of monoclonal antibodies and Indocayanine Green," *Cancer Res.* **69**(4), 1268–1272 (2009).